International Journal of Heat and Mass Transfer 53 (2010) 3839–3846

Contents lists available at ScienceDirect

International Journal of Heat and Mass Transfer

journal homepage: www.elsevier.com/locate/ijhmt

Effect of wall roughness on shear viscosity and diffusion in nanochannels

F. Sofos, T.E. Karakasidis *, A. Liakopoulos

Hydromechanics and Environmental Engineering Laboratory, School of Engineering, University of Thessaly, 38834 Pedion Areos, Volos, Greece

ARTICLE INFO

Article history:
Received 8 May 2009
Available online 4 June 2010

Keywords:
NEMD simulation
Diffusion coefficient
Shear viscosity
Transport properties
Rough wall nanochannels

ABSTRACT

The effect of wall roughness on liquid argon shear viscosity and diffusion coefficient in nanochannels is studied by non-equilibrium molecular dynamics. Diffusion coefficient results are presented in terms of average values for the whole channel, as well as profiles of local values calculated in layers along the channel. It turns out that the local diffusion coefficient decreases significantly in fluid layers adjacent to the rough wall due to the trapping of fluid atoms inside the rough wall cavities. The degree of anisotropy in the *x*-, *y*- and *z*-components of the diffusion coefficient close to the rough wall increases relative to the anisotropy observed close to the smooth wall. Stress tensor components as well as local strain rates are evaluated in order to extract the coefficient of shear viscosity, η_s, which presents significant variations near the rough wall. These results should be taken into consideration when it comes to the design of nanofluidic devices.

1. Introduction

The importance of channel width in channel flows at the nanoscale has been discussed in great detail in the literature [1–10]. For small channel widths, the fluid is inhomogeneous near the solid boundary and Navier–Stokes-based hydrodynamic prediction of the velocity profile and the no-slip condition break down. Non-equilibrium molecular dynamics (NEMD) offers an effective alternative simulation method for flow systems at the nanoscale and simultaneously provides a valuable method for the calculation of transport properties of liquids.

Calculation of the diffusion coefficient of fluids at the nanoscale for flat-wall nanochannels has been addressed by many researchers [11,12]. A useful review on diffusivity issues in slit pores in [2] shows that mobility is maintained even in pore widths of 2.0σ (σ is a length-scale parameter depending on interatomic interactions). In a previous work for argon flow in krypton nanochannels [13] we found that diffusivity is anisotropic in small channels with flat walls while isotropic diffusion is reached for channels of width greater than about 20σ. Moreover, diffusion coefficient is higher in layers close to the center of the channel and decreases in layers adjacent to the walls. As the channel width increases bulk-like behavior is approached close to the centerline.

As far as shear viscosity is concerned, a number of computational studies by equilibrium or non-equilibrium MD have been reported in the literature for flat-wall nanochannels. For systems close to equilibrium, the Green–Kubo (GK) method is preferred [13–17], though it demands complex calculations and significant simulation time in order to give statistically accurate results. However, in systems confined between solid walls, if one takes into account the induced strain rates, NEMD methods for the calculation of shear viscosity are a good alternative [6,7,18–21].

The effect of wall structure on fluid properties is currently an intriguing subject in the area of nanofluidics. Many researchers have dealt with the effect of roughness on flow and slip at the boundary [22–27]. Fluid atom localization near a rough wall is of particular interest, since there is clear evidence of fluid atom trapping inside the wall interstices, as it was shown in [28], and this is expected to affect to some degree transport properties of fluids. As far as diffusion coefficient is concerned, Kim and Darve [29] found that diffusion coefficient decreases near a rough channel wall in electro-osmotic flow of water molecules through channels with rectangular roughness. On the other hand, in [27] it is reported that fluid viscosity increases as the roughness height increases and as the roughness period decreases.

It would be of great interest to investigate in detail diffusivity and shear viscosity issues in channels with walls that present a kind of structural anomaly, especially in fluid layers adjacent to those anomalies. In the present work, we simulated liquid argon flow in a channel with one smooth and one rough wall, where the rough wall is formed by periodically spaced rectangular protrusions. The calculation of the diffusion coefficient and shear viscosity will shed further light on the phenomena occurring and affecting flow and mass transport close to a rough surface.

The present paper is set up as follows. Section 2 contains the molecular model and the method of computing transport properties, while in Section 3 results are presented and discussed. Finally, Section 4 contains concluding remarks.

* Corresponding author. Tel.: +30 2421074163; fax: +30 2421074169.
E-mail address: thkarak@uth.gr (T.E. Karakasidis).

0017-9310/$ - see front matter © 2010 Elsevier Ltd. All rights reserved.
doi:10.1016/j.ijheatmasstransfer.2010.04.037

Nomenclature

D	diffusion coefficient, $D = \frac{D_x+D_y+D_z}{3}$
D_{lay}	diffusion coefficient value in a specific layer along the channel
F_{ext}	external driving force (magnitude)
h	channel width
K	spring constant
k_B	Boltzmann constant
L_x	length of the computational domain in the x-direction
L_y	length of the computational domain in the y-direction
L_z	length of the computational domain in the z-direction
l_g	protrusion or cavity length
m	argon atom mass
MSD	mean square displacement
N	number of atoms
p	periodic roughness factor
$\mathbf{P}$	microscopic stress tensor
$\mathbf{P}^{kin}$	kinetic part of the stress tensor
$\mathbf{P}^{pot}$	potential energy part of the stress tensor
$P_{off\text{-}diag}$	average of all three independent off-diagonal elements of the stress tensor, $P_{off\text{-}diag} = \frac{P_{xz}+P_{xy}+P_{yz}}{3}$
r_{eq}	position of a wall atom on fcc lattice site
$\mathbf{r}_i$	position vector of atom i
$\mathbf{r}_{ij}$	distance vector between ith and jth atom
T	temperature
v^i	ith component of atomic velocity, $i = 1, 2, 3$
$u(\mathbf{r}_{ij})$	LJ potential of atom i with atom j
V	volume of the computational domain ($L_x \times L_y \times L_z$)

Greek symbols

$\dot{\gamma}$	shear rate
ε	energy parameter in the LJ potential
η_s	shear viscosity
σ	length parameter in the LJ potential

2. Simulation method

2.1. Molecular model

Non-equilibrium molecular dynamics simulations were performed to simulate flow of liquid argon in a channel with krypton walls. The lower wall of the channel is smooth. The rough upper wall is constructed by "adding" extra wall atoms to form periodically spaced rectangular protrusions (see Fig. 1). We considered four different cases of upper wall roughness ($p = 1$, 2, 3 and 6, as shown schematically in Fig. 1), where p represents the number of rectangular grooves in the computational domain, i.e., $p = 1$ signifies one rectangular groove, $p = 2$ two rectangular grooves, $p = 3$ three rectangular grooves and $p = 6$ six rectangular grooves. We refer to the flat-wall nanochannel as case $p = 0$. The dimensions of the computational domain in x-, y- and z-directions are $L_x \times L_y \times L_z = 10.6 \times 10.6 \times 23$ (in units of σ which is defined below). Roughness height is about 2σ (or, 10% of the channel width) and the protrusion length (and, equivalently, the cavity length) l_g equals to $L_x/2p$ (i.e., $l_g = 5.3$, 2.65, 1.77 and 0.88σ for $p = 1$, 2, 3 and 6, respectively).

Fluid/fluid, fluid/wall and wall/wall atom interactions are described by the Lennard-Jones (LJ) 12-6 potential

$$u^{LJ}(r_{ij}) = 4\varepsilon\left((\sigma/r_{ij})^{12} - (\sigma/r_{ij})^{6}\right) \quad (1)$$

where the parameters of the Lennard-Jones potential are: $\sigma_{Ar-Ar} = 0.3405$ nm (from now on σ_{Ar-Ar} will be referred as σ), $\sigma_{Kr-Kr} = 0.3633$ nm, $\sigma_{Ar-Kr} = 0.3519$ nm, $\varepsilon_{Ar-Ar}/k_B = 119.8$ K (from now on will be referred as ε), $\varepsilon_{Kr-Kr}/k_B = 167.0$ K, $\varepsilon_{Ar-Kr}/k_B = 141.4$ K, the atomic mass for argon is $m_{Ar} = 39.95$ a.u. (from now on will be referred as m), the atomic mass for krypton is $m_{Kr} = 83.8$ a.u. and the cut-off radius is $r_c = 2.5\sigma$. Periodic boundary conditions are considered in x- and y-directions. Each rough wall channel consists of 504 wall atoms and 1368 fluid atoms. Wall atoms are bound on fcc sites and remain approximately at their original positions due to the effect of an elastic spring force $\mathbf{F} = -K(\mathbf{r}(t) - \mathbf{r}_{eq})$, where $\mathbf{r}(t)$ is the vector position of a wall atom at time t, $\mathbf{r}_{eq}$ is its initial lattice position vector and $K = 57.15$ (ε/σ^2) is the wall spring constant [18]. Temperature is kept constant at $T^* = 1$ (ε/k_B, k_B is the Boltzmann's constant) with the application of appropriate Nosé–Hoover thermostats. An external driving force $F_{ext} = 0.01344$ (ε/σ) is applied along the x-direction to drive the flow.

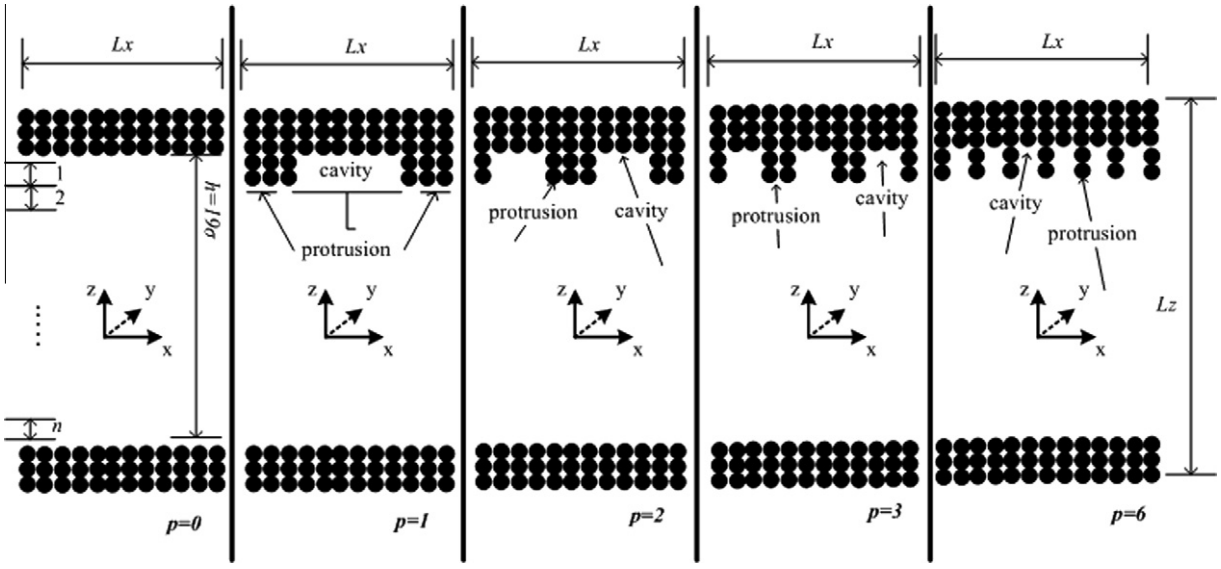

Fig. 1. Schematic of channel models. Also shown layers used for the calculations of local transport properties. Channel dimensions are $-5.3\sigma \leqslant x \leqslant 5.3\sigma$, $-5.3\sigma \leqslant y \leqslant 5.3\sigma$ and $-11.5\sigma \leqslant z \leqslant 11.5\sigma$.

The simulation step is $\Delta t = 0.005\tau$ (τ is in units of $\sqrt{m\sigma^2/\varepsilon}$). In the beginning, fluid atoms are given appropriate initial velocities in order to reach the desired temperature ($T^* = 1$). The system reaches equilibrium state after a run of 2×10^6 time steps. Then, typically 10 NEMD simulations are performed, each with duration of 5×10^5 time steps, in order to obtain statistically accurate results.

2.2. Computation of transport properties

The diffusion coefficient can be obtained using either Einstein's relation

$$D = \lim_{t\to\infty} \frac{1}{2dNt} \left\langle \sum_{j=1}^{N} \left[\mathbf{r}_j(t) - \mathbf{r}_j(0)\right]^2 \right\rangle \tag{2}$$

or Green–Kubo's relation

$$D = \frac{1}{3N} \int_0^\infty \left\langle \sum_{j=1}^{N} \mathbf{v}_j(0) \cdot \mathbf{v}_j(t) \right\rangle \tag{3}$$

where $\mathbf{r}_j$ is the position vector of the jth atom and d is the dimensionality of the system ($d = 1$ for diffusivity calculation in one direction, $d = 2$ in two directions and $d = 3$ in three directions) and $\mathbf{v}_j$ denotes the velocity vector of the jth atom.

The two relations are equivalent and provide the same results [1,2]. Relations (2) and (3) are derived for systems in equilibrium, but they can be used for non-equilibrium systems as well, provided one excludes the drift contribution from the flow [2]. In the present work, we have used Einstein's relation for the calculation of the diffusion coefficient. The computation is carried out in two steps. In the first step, the mean square displacement (MSD) is obtained from the definition

$$\mathrm{MSD}(t) = \frac{1}{N} \left\langle \sum_{j=1}^{N} \left[\mathbf{r}_j(t) - \mathbf{r}_j(0)\right]^2 \right\rangle \tag{4}$$

and subsequently D is evaluated based on Eq. (2) which can be written as

$$D = \lim_{t\to\infty} \frac{1}{2dt} \mathrm{MSD}(t) \tag{5}$$

The channel diffusion coefficient calculated as an average value over the whole channel region is defined as

$$D_{\mathrm{ch}} = \lim_{t\to\infty} \frac{1}{6t} \mathrm{MSD}(t) \tag{6}$$

while the channel diffusion coefficient calculated in x-, y- and z-components, is

$$D_i = \lim_{t\to\infty} \frac{1}{2t} \mathrm{MSD}_i(t) \tag{7}$$

where $i = x$, y or z, and, finally

$$D_{\mathrm{ch}} = \frac{D_x + D_y + D_z}{3} \tag{8}$$

Moreover, the channel is divided into n bins (or, layers) in the z-direction, each one of volume $V_{\mathrm{lay}} = L_x \times L_y \times (h/n)$ (see Fig. 1), and the diffusion coefficients are also calculated as local values in these layers as

$$D_{i,\mathrm{lay}} = \lim_{t\to\infty} \frac{1}{2t} \mathrm{MSD}_{i,\mathrm{lay}}(t) \tag{9}$$

where $i = x$, y or z and $n = 6$. Notice that $\mathrm{MSD}_{i,\mathrm{lay}}(t)$ is the local mean value in every bin. More precisely each atom is taken into account only for the time that it is located inside the corresponding bin. When an atom leaves the bin it is not taken into account in the calculation of MSD of this bin, while new atoms that enter the bin are taken into account in the MSD calculation as long as they remain inside the bin.

As a three-component average in each channel layer, the diffusion coefficient is

$$D_{\mathrm{lay}} = \frac{D_{x,\mathrm{lay}} + D_{y,\mathrm{lay}} + D_{z,\mathrm{lay}}}{3} \tag{10}$$

Shear viscosity in confined nanochannels can be calculated by NEMD or Green–Kubo relations. Green–Kubo methods are mainly used in systems close to or at equilibrium state and they do not take into account the induced strain rates, while NEMD methods do. In the present work, NEMD methods have been chosen due to the existence of wall roughness which affects fluid behavior and induces non-linear strain rates, as shown in Section 3.

Shear viscosity is also evaluated as local value at various layers across the z-direction of the channels, each one of volume $V_{\mathrm{lay}} = L_x \times L_y \times (h/n)$, where $n = 40$. Shear viscosity $\eta_s(z)$ across the z-direction for a pure fluid is computed by the relation

$$\eta_s(z) = \lim_{F_{\mathrm{ext}}\to 0} \left[-\frac{\langle P_{xz}(z)\rangle}{\dot{\gamma}(z)} \right] \tag{11}$$

where the strain rate $\dot{\gamma}(z)$ is

$$\dot{\gamma}_{xz} = \frac{\partial v_x}{\partial z} + \frac{\partial v_z}{\partial x} \tag{12}$$

For flat channel walls, the second term in Eq. (12) is negligible (in the macroscale, the second term in Eq. (12) is identically zero) thus the first term of Eq. (12) is the dominant one and taken into account in the calculations. However, since adjacent to the rough wall, the flow field can be distorted by the cavities, i.e., the fluid velocity is not parallel to the x-axis we have performed detailed calculations of the average strain rate components inside the cavity. These calculations showed that $\frac{\partial v_z}{\partial x}$ is a very small part of the strain rate (less than 8%). Far from the rough wall, differences between $\dot{\gamma}_{xz}$ and $\frac{\partial v_x}{\partial z}$ are even far less significant. Summarizing, the effect on the calculated viscosity value is small when we neglect the second term of Eq. (12), even when we are inside the cavity. Thus the viscosity calculations have been performed taking into account only the first term in the right-hand side of Eq. (12).

$P_{xz}(z)$ is the off-diagonal component of the microscopic stress tensor $\mathbf{P}$, and $\langle\cdots\rangle$ denotes time-averaged values. P_{xz} is given by

$$P_{xz} = \frac{1}{V_{\mathrm{bin}}} \left(\sum_{i=1}^{N} m_i v_i^x v_i^z - \sum_{i=1}^{N} \sum_{j>1}^{N} r_{ij}^x \frac{\partial u(r_{ij})}{\partial r_{ij}^z} \right) \tag{13}$$

where $u(r_{ij})$ is the LJ potential of atom i interacting with atom j, r_{ij} is the distance between atoms i and j, and v_i^j is the j-component ($j = x$, y or z) of the velocity of atom i (the mean flow velocity is subtracted from v_i^x). The above expression for the stress tensor can be separated in a kinetic and a potential energy parts. We denote the kinetic part of the stress tensor by P_{xz}^{kin}, i.e.,

$$P_{xz}^{\mathrm{kin}} = \sum_{i=1}^{N} m_i v_i^x v_i^z \tag{14}$$

and the potential energy part by P_{xz}^{pot}, i.e.,

$$P_{xz}^{\mathrm{pot}} = \sum_{i=1}^{N} \sum_{j>1}^{N} r_{ij}^x \frac{\partial u(r_{ij})}{\partial r_{ij}^z} \tag{15}$$

With definitions (14) and (15), Eq. (13) can be rewritten as

$$P_{xz} = \frac{1}{V_{\mathrm{bin}}} \left(P_{xz}^{\mathrm{kin}} - P_{xz}^{\mathrm{pot}} \right) \tag{16}$$

In order to obtain better statistics and more accurate results for the stress tensor, we calculate all three independent off-diagonal elements of the stress tensor and average them as suggested in [30], i.e.,

$$P_{\text{off-diag}} = \frac{P_{xz} + P_{xy} + P_{yz}}{3} \tag{17}$$

Finally, in our computations, Eq. (11) becomes

$$\eta_s(z) = \lim_{F_{\text{ext}} \to 0} \left[-\frac{\langle P_{\text{off-diag}}(z) \rangle}{\dot{\gamma}(z)} \right] \tag{18}$$

3. Results and discussion

3.1. Diffusion coefficient

In order to calculate the diffusion coefficient we need to calculate first the mean square displacement of fluid atoms, according to Eq. (4), and then evaluate the slope of the corresponding diagrams following Eq. (5). We present MSD_{lay} diagrams (in six layers, L1–L6, see Fig. 1) for each rough channel considered in Fig. 2(a)–(d). In Fig. 2(a), we depict MSD_{lay} for $p = 1$. We observe that the slopes of L1 (channel layer adjacent to the lower smooth wall) and L6 (channel layer adjacent to the upper rough wall) are significantly smaller compared to the respective slopes of the interior channel layers (L2–L5). This is also the trend for all other rough channels (Fig. 2(b)–(d)), since MSD_{lay} in all channel layers, except L6, is similar in every channel ($p = 1$, 2, 3 and 6). However, we observe that the slope at L6 (layer close adjacent to the rough wall) decreases as p increases and consequently the corresponding diffusion coefficient values will also decrease.

We present calculated D_{lay} values in Fig. 3(a). In general, the diffusion coefficient has smaller values in fluid regions close to the solid boundary compared to fluid regions in the interior of the channel [2,13]. Furthermore, in all our calculations in the present work, the rate of diffusion is even smaller in fluid layers adjacent to the rough wall compared to rate close to the smooth wall and this can be attributed to the fact that a number of fluid atoms are trapped inside the rectangular cavities [28] and their movement is considerably obstructed. Moreover, as p increases, the diffusion coefficient near the rough wall decreases. This can be attributed to the fact that the trapping time of fluid atoms inside the cavities increases as the parameter p increases

The diffusion coefficient component ratio $\frac{D_{z,\text{lay}}}{D_{x,\text{lay}}}$ (or, equivalently, $\frac{D_{z,\text{lay}}}{D_{y,\text{lay}}}$) is depicted in Fig. 3(b). We observe that although only a slight anisotropy is present near the smooth wall, near the rough walls, the ratio $\frac{D_{z,\text{lay}}}{D_{x,\text{lay}}}$ increases considerably as p increases, and diffusivity becomes highly anisotropic. This is due to the fact that fluid atom mobility is reduced inside the roughness cavities [28], which leads to the reduction of $D_{x,\text{lay}}$ in these regions.

In the diagram of D_{ch} values (see Eq. (8)), in Fig. 4, diffusion coefficient has a slightly decaying behavior as p increases. This result is in agreement with the results in [28] and supports the

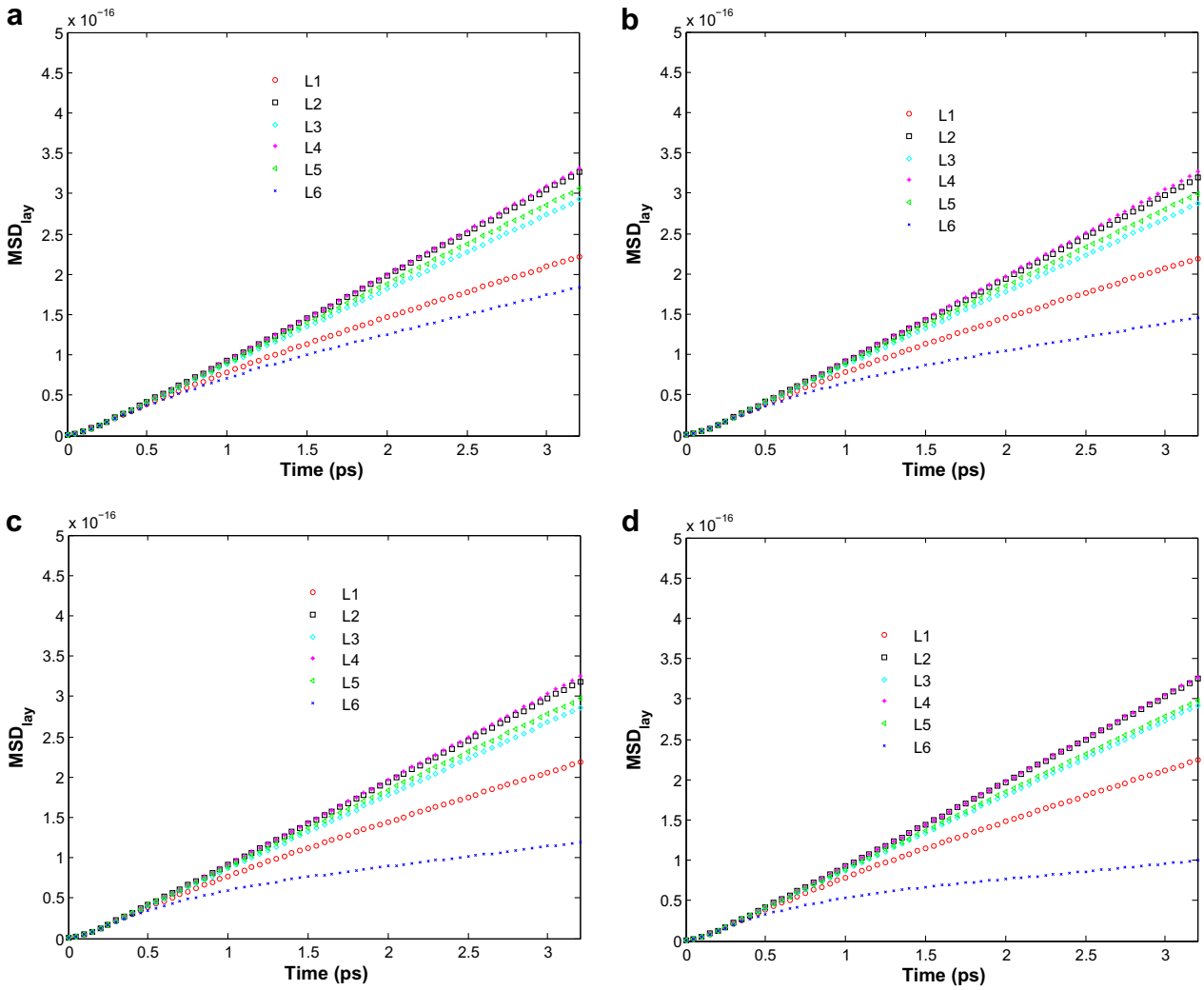

Fig. 2. Mean square displacement calculated in layers along the channels for (a) $p = 1$, (b) $p = 2$, (c) $p = 3$ and (d) $p = 6$.

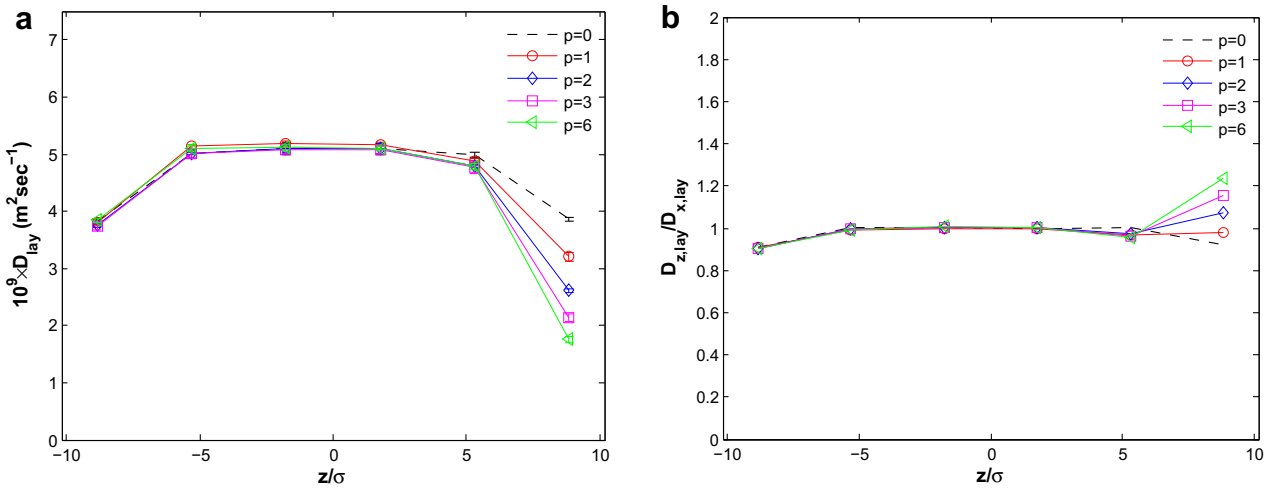

Fig. 3. Diffusion coefficient as (a) $D_{lay} = \frac{D_{x,lay}+D_{y,lay}+D_{z,lay}}{3}$ and (b) component ratio $D_{z,lay}/D_{y,lay}$ (or, equivalently, $D_{z,lay}/D_{x,lay}$). Lines are guide to the eye.

observation of increasingly strong trapping of fluid atoms inside the cavities as p increases from 0 to 6 (i.e., as the length of protrusion decreases).

Summarizing, in the present work we simulated a hydrophilic like surface since the interaction parameters ratio between wall/fluid atoms is $\varepsilon_{wall}/\varepsilon_{fluid} = 1.2$ (see also [10]). In a recent paper [28] where a similar channel geometry with hydrophilic surfaces ($\varepsilon_{wall}/\varepsilon_{fluid} = 1.2$) was employed, it was found that increasing p results in increased trapping time of atoms inside the cavities, which in turn can explain that the resulting MSD of the atoms close to the rough wall decreases and thus the calculated diffusion coefficient is reduced. In [28] it was also found that the slip length decreases as p increases, which is in accordance with the general trend relating slip length and diffusion coefficient discussed in [31]. On the other hand, one can reasonably expect that in the case of hydrophobic surface walls, a different behavior would be observed since the hydrophobic interactions would not favor increased trapping time of atoms, and thus would affect less the MSD of atoms and the corresponding diffusion coefficient. Thus we believe that, as mentioned in [31], the surface roughness in combination with the type of interactions (hydrophibic/hydrophilic) can significantly affect the fluid behavior as discussed in detail in [31] and worth's further research.

3.2. Shear viscosity

To calculate the shear viscosity, we first evaluate the strain rate $\dot{\gamma}(z)$ and the stress tensor component $P_{off\text{-}diag}(z)$ in protrusions and cavities (as average values across z-dimension, see Fig. 5), and then extract shear viscosity values according to Eq. (11). Furthermore, we decompose $P_{off\text{-}diag}(z)$ in its kinetic $P^{kin}_{off\text{-}diag}$ and potential part $P^{pot}_{off\text{-}diag}$ according to Eqs. (14) and (15) in order to determine which component affects more the final result.

We calculate all three off-diagonal stress tensor components and strain rates for each channel ($p = 1$, 2, 3 and 6) and present the results for $p = 1$ in Fig. 6(a)–(d). In Fig. 6(a) and (b), we present $P^{kin}_{off\text{-}diag}$ and $P^{pot}_{off\text{-}diag}$, respectively, as functions of z. As far as the kinetic part of the stress tensor components $\left(P^{kin}_{off\text{-}diag}\right)$ is concerned, it has clearly smaller values across the channel compared to the potential component $P^{pot}_{off\text{-}diag}$, both at channel cavities and protrusions. As a result, the potential part is the one that basically determines the value of the stress tensor component $P_{off\text{-}diag}(z)$ shown in Fig. 6(c).

We also observe that near the rough wall protrusions, $P^{pot}_{off\text{-}diag}$ presents a sharp increase. This may be attributed to the fact that the potential energy is higher in these regions compared to channel regions far from the walls, as shown in [28]. In Fig. 6(d) the strain rate, $\dot{\gamma}(z)$, for $p = 1$ is depicted. The strain rate would be a lin-

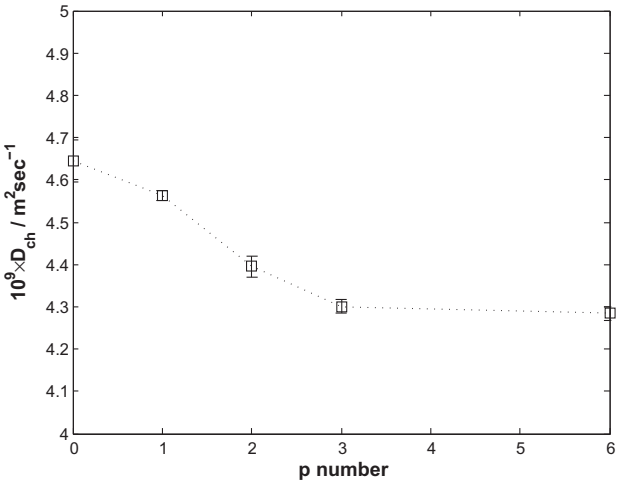

Fig. 4. Channel diffusion coefficient as a function of p. Dotted line is a guide for the eye.

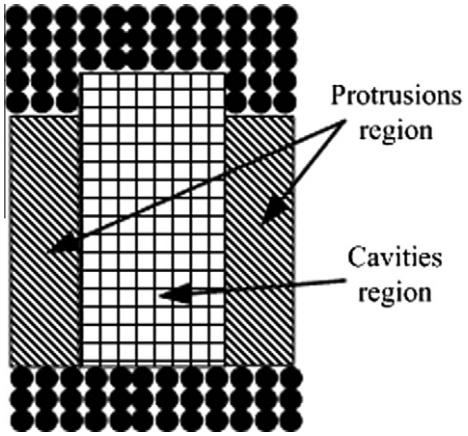

Fig. 5. Schematic of the $p = 1$ channel, where it is shown how the spatial averaging of $P_{off\text{-}diag}(z)$, $\dot{\gamma}(z)$ and $\eta_s(z)$ is made across the z-direction of the protrusions and cavities. Similar averaging is done for $p = 2$, 3 and 6.

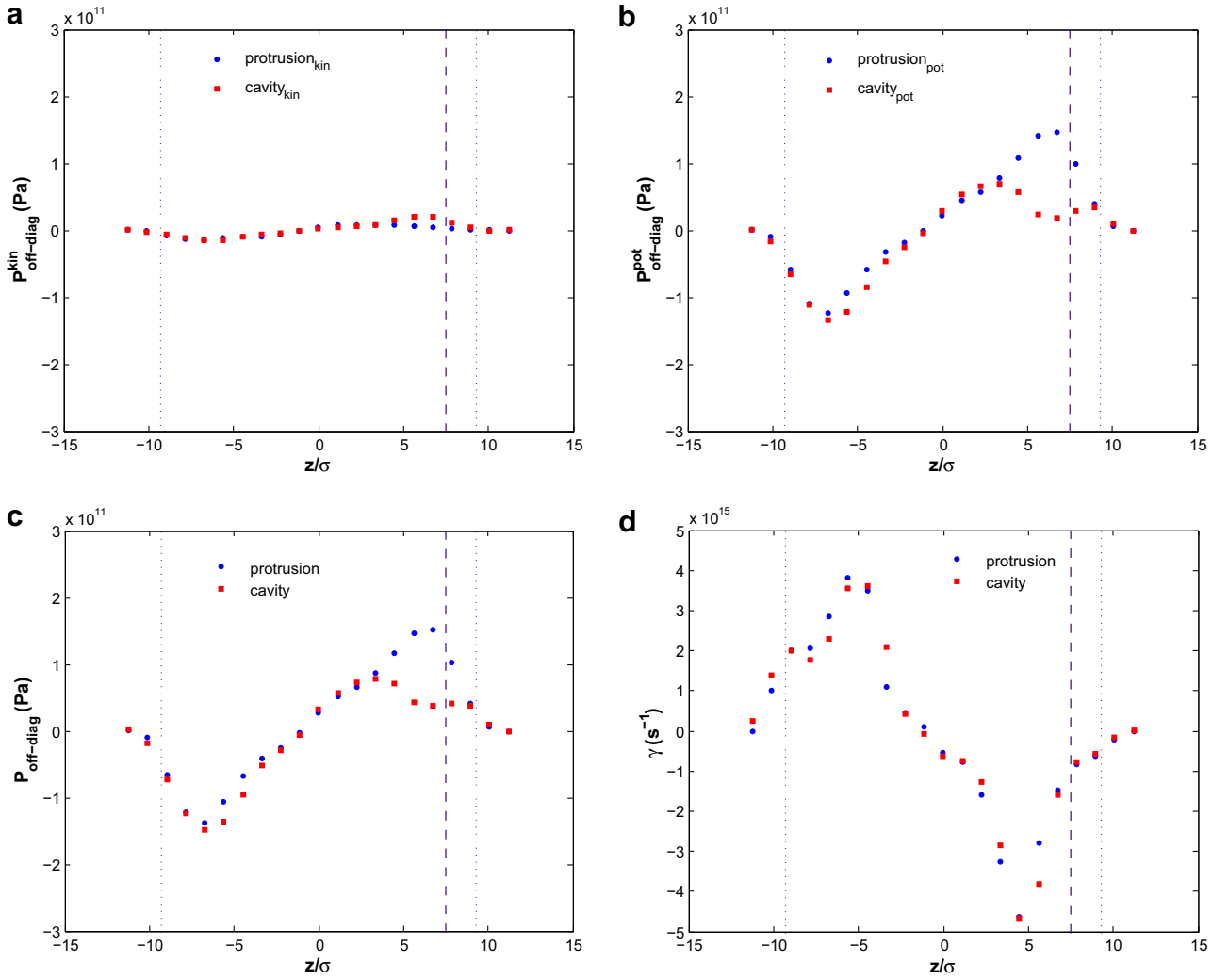

Fig. 6. $p = 1$. (a) The kinetic part $P^{kin}_{off\text{-}diag}$, Eq. (14); (b) the potential part $P^{pot}_{off\text{-}diag}$, Eq. (15). (c) $P_{off\text{-}diag}$, Eq. (17) and (d) strain rate $\dot{\gamma}$. Dotted lines denote wall limits and dashed lines the protrusion limits.

ear function of z, if the respective velocity profile is locally parabolic [10]. However, in [28] we found that the velocity profile near a rough wall can not be parabolically fitted for any p value. Consequently, we observe that there exist strong deviation from linearity for $\dot{\gamma}(z)$ near the walls and, especially, close to the rough wall. Since we found that velocity profiles are quite similar both at cavities and protrusions [28], as a consequence, we also observe that the strain rate profiles are similar, too.

Applying Eq. (18) to calculated values of $P_{off\text{-}diag}(z)$ and $\dot{\gamma}(z)$, we obtain the shear viscosity profiles shown in Fig. 7(a)–(d), for $p = 1$, 2, 3 and 6, respectively. The profiles reveal interesting information on shear viscosity behavior, especially near the rough wall. All profiles are not symmetric with respect to plane $z = 0$ due to the existence of protrusions. For any $z = const.$, η_s at the protrusions is always greater than η_s at the cavities. For $p = 1$ (Fig. 7(a)), we observe that shear viscosity presents its lowest values inside the cavities. On the contrary, we obtain the highest shear viscosity values at the protrusions. This behavior may be attributed to the interaction of the fluid with the walls which at the nanoscale becomes important, especially in the cavity region, as it was revealed by the shape of the potential energy maps of the fluid atoms in [28]. For $p = 2$ (Fig. 7(b)), shear viscosity has similar behavior to $p = 1$ at the cavities, but with higher values at the protrusions. For $p = 3$ and 6 (Fig. 7(c) and (d), respectively) the shear viscosity profiles are similar to $p = 1$.

We present channel shear viscosity as a function of p in Fig. 8. Shear viscosity values for $p = 0$ (the smooth or flat-wall channel) is taken from [13]. We observe that η_s is higher for all rough wall channels compared to the flat-wall channel and, furthermore, the channel shear viscosity does not increase monotonically as p increases, a behavior also reported in [27].

4. Conclusions

We have presented non-equilibrium molecular dynamics simulations of liquid argon flow in nanochannels characterized by periodic rectangular wall roughness. The effect of protrusion length (or, equivalently, cavity length) on diffusion coefficient and shear viscosity is found to be significant and should be taken into account in the design of nanofluidic systems, since it affects both flow and mass transfer.

The channel diffusion coefficient, D_{ch}, decreases slightly as cavities become narrower. Moreover, the local diffusion coefficient is smaller near a rough wall compared to a smooth wall. The presence of solid walls generally induces anisotropy adjacent to the walls, but, anisotropy increases near a rough wall. As wall cavities become narrower, the ratio of local diffusion coefficient components $\frac{D_{z,lay}}{D_{x,lay}}$ increases, fluid mobility in the x-direction near the rough wall decreases, and $D_{x,lay}$ decreases.

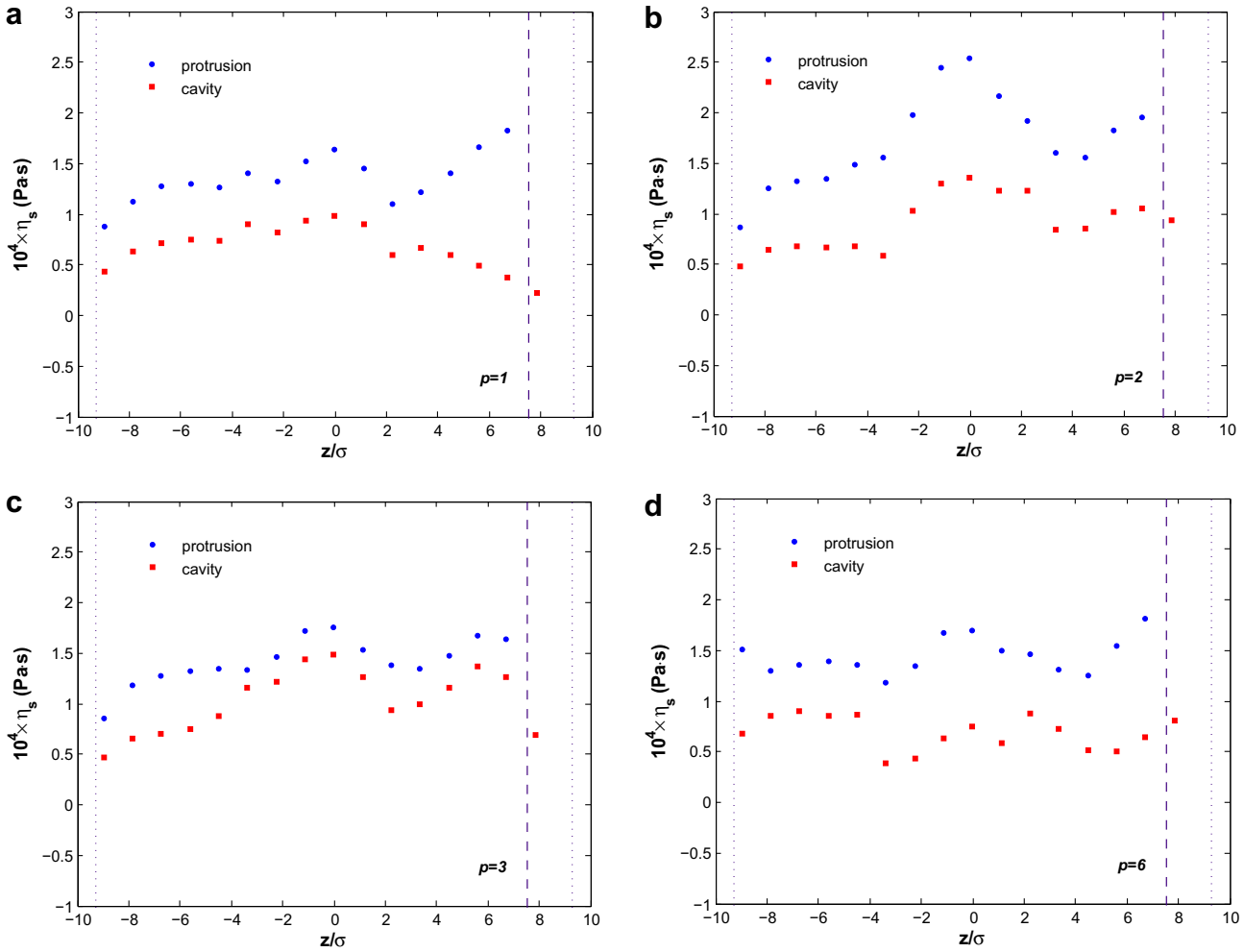

Fig. 7. Shear viscosity profiles at cavities and protrusions for (a) $p = 1$, (b) $p = 2$, (c) $p = 3$ and (d) $p = 6$. Dotted lines denote the lower wall limits and dashed lines the protrusion limits.

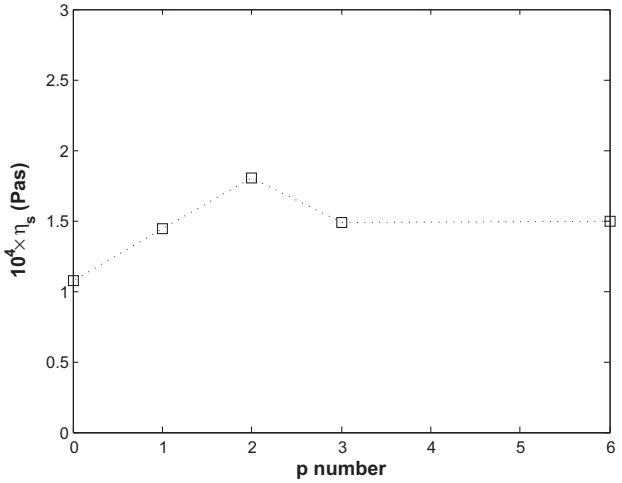

Fig. 8. Channel shear viscosity as function of p (or, equivalently, protrusion length).

The calculations of the off-diagonal components of the stress tensor, as well as the strain rate profiles have been used for the calculation of shear viscosity profiles across each channel studied. Strain rates are higher close to the rough wall and deviate from a linear profile, since the respective velocity profiles can not be parabolically fitted. Stress tensor components across the channel protrusions have greater values compared to cavities, and, as a result, shear viscosity profiles present slightly higher values at the protrusions. In general, we found that channel shear viscosity is higher in rough wall nanochannels compared to flat wall.

The existence of wall roughness in almost all real materials, either due to the atomic localization or due to surface anomalies, is a feature that has to be studied extensively when it comes to designing flow systems at the nanoscale with tailored properties. Depending on the surface, a number of fluid atoms are trapped inside the wall interstices and this affects flow properties, shear viscosity and rates of diffusion of liquids.

Acknowledgements

This research project (PENED-uth-3337C) is co-financed by E.U.-European Social Fund (75%) and the Greek Ministry of Development-GSRT (25%).

References

[1] D.C. Rapaport, The Art of Molecular Dynamics Simulation, Cambridge University Press, Cambridge, 1995.
[2] G.E. Karniadakis, A. Beskok, N. Aluru, Microflows and Nanoflows: Fundamentals and Simulation, Springer, Berlin, 2002.
[3] K. Binder, J. Horbach, W. Kob, W. Paul, F. Varnik, Molecular dynamics simulations, J. Phys.: Condens. Matter 16 (2004) 429–453.

[4] J. Koplik, J.R. Banavar, J.F. Willemsen, Molecular dynamics of fluid flow at solid surfaces, Phys. Fluids A 1 (5) (1989) 781–794.
[5] U. Heinbuch, J. Fischer, Liquid flow in pores: slip, no-slip, or multilayer sticking, Phys. Rev. A 40 (2) (1989) 1144–1146.
[6] K.P. Travis, B.D. Todd, D.J. Evans, Departure from Navier–Stokes hydrodynamics in confined liquids, Phys. Rev. E 55 (4) (1997) 4288–4295.
[7] K.P. Travis, K.E. Gubbins, Poiseuille flow of Lennard-Jones fluids in narrow slit pores, J. Chem. Phys. 112 (4) (2000) 1984–1994.
[8] J. Delhommele, D.J. Evans, Configurational temperature profile in confined liquids. I. Atomic fluid, J. Chem. Phys. 114 (14) (2001) 6229–6235.
[9]] J. Delhommele, D.J. Evans, Configurational temperature profile in confined liquids. II. Molecular fluids, J. Chem. Phys. 114 (14) (2001) 6236–6241.
[10] F. Sofos, T. Karakasidis, A. Liakopoulos, Non-equilibrium molecular dynamics investigation of parameters affecting planar nanochannel flows, Contemp. Eng. Sci. 2 (6) (2009) 283–298.
[11] I. Bitsanis, J.J. Magda, M. Tirell, H.T. Davis, Molecular dynamics of flow in micropores, J. Chem. Phys. 87 (3) (1987) 1733–1750.
[12] S. Murad, P. Ravi, J.G. Powles, A computer simulation study of fluids in model slit, tubular, and cubic micropores, J. Chem. Phys. 98 (12) (1993) 9771–9781.
[13] F. Sofos, T. Karakasidis, A. Liakopoulos, Transport properties of liquid argon in krypton nanochannels: anisotropy and non-homogeneity introduced by the solid walls, Int. J. Heat Mass Transfer 52 (2) (2009) 735–743.
[14] K. Meier, A. Laesecke, S. Kabelac, A molecular dynamics simulation study of the self-diffusion coefficient and viscosity of the Lennard-Jones fluid, Int. J. Thermophys. 22 (1) (2001) 161–173.
[15] Y. Yonetani, K. Kinugawa, Centroid molecular dynamics approach to the transport properties of liquid para-hydrogen over the wide temperature range, J. Chem. Phys. 120 (22) (2004) 10624–10633.
[16] H.L. Song, K.P. Dong, B.K. Dae, Molecular dynamics simulations for transport coefficients of liquid argon: new approaches, Bull. Korean Chem. Soc. 24 (2) (2003) 178–182.
[17] M.F. Pas, B.J. Zwolinski, Computation of the transport coefficients of dense fluid neon, argon, krypton and xenon by molecular dynamics, Mol. Phys. 73 (3) (1991) 471–481.
[18] S.Y. Liem, D. Brown, J.H.R. Clarke, Investigation of the homogeneous-shear non-equilibrium-molecular-dynamics method, Phys. Rev. A 45 (6) (1992) 3706–3713.
[19] B.D. Todd, D.J. Evans, P.J. Daivis, Pressure tensor for inhomogeneous fluids, Phys. Rev. E 52 (2) (1995) 1627–1638.
[20] E. Akhmatskaya, B.D. Todd, P. J Daivis, D.J. Evans, K.E. Gubbins, L.A. Pozhar, A study of viscosity inhomogeneity in porous media, J. Chem. Phys. 106 (11) (1997) 4684–4695.
[21] K. Singer, J.V.L. Singer, D. Fincham, Determination of the shear viscosity of atomic liquids by non-equilibrium molecular dynamics, Mol. Phys. 40 (2) (1980) 515–519.
[22] G. Mo, F. Rosenberger, Molecular dynamics simulation of flow in two-dimensional channel with atomically rough walls, Phys. Rev. A 42 (1990) 4688–4692.
[23] N.V. Priezjev, Effect of surface roughness on rate-dependent slip in simple fluids, J. Chem. Phys. 127 (2007) 144708.
[24] T.M. Galea, P. Attard, Molecular dynamics study of the effect of atomic roughness on the slip length at the fluid–solid boundary during shear flow, Langmuir 20 (2004) 3477–3482.
[25] B.Y. Cao, M. Chen, Z.Y. Guo, Liquid flow in surface-nanostructured channels studied by molecular dynamics simulation, Phys. Rev. E 74 (2006) 066311.
[26] A.S. Ziarani, A.A. Mohammad, Molecular dynamics study of velocity slip in microchannels, in: R. Wamkeue (Ed.), Proceedings of the 17th IASTED International Conference Modelling and Simulation, ACTA Press, Montreal, QC, 2006, pp. 585–590.
[27] A. Jabbarzadeh, J.D. Atkinson, R.I. Tarner, Effect of the wall roughness on slip and rheological properties of hexadecane in molecular dynamics simulation of Couette shear flow between two sinusoidal walls, Phys. Rev. E 61 (1) (2000) 690–699.
[28] F. Sofos, T. Karakasidis, A. Liakopoulos, Effects of wall roughness on flow in nanochannels, Phys. Rev. E 79 (2009) 026305.
[29] D. Kim, E. Darve, Molecular dynamics simulation of electro-osmotic flows in rough wall nanochannels, Phys. Rev. E 73 (2006) 051203–051212.
[30] G.A. Fernandez, J. Vrabec, H. Hasse, A molecular simulation study of shear and bulk viscosity and thermal conductivity of simple real fluids, Fluid Phase Equilib. 221 (2004) 157–163.
[31] B.Y. Cao, J. Sun, M. Chen, Z.-Y. Guo, Molecular momentum transport at fluid–solid interface in MEMS/NEMS: a review, Int. J. Mol. Sci. 10 (2009) 4638.